A&A 642, L17 (2020)
https://doi.org/10.1051/0004-6361/202039351

Astronomy & Astrophysics

LETTER TO THE EDITOR

Discovery of HC_3O^+ in space: The chemistry of O-bearing species in TMC-1⋆

J. Cernicharo[1], N. Marcelino[1], M. Agúndez[1], Y. Endo[2], C. Cabezas[1], C. Bermúdez[1], B. Tercero[3,4], and P. de Vicente[4]

[1] Grupo de Astrofísica Molecular, Instituto de Física Fundamental (IFF-CSIC), C/ Serrano 121, 28006 Madrid, Spain
e-mail: jose.cernicharo@csic.es
[2] Department of Applied Chemistry, Science Building II, National Chiao Tung University, 1001 Ta-Hsueh Rd., Hsinchu 30010, Taiwan
[3] Observatorio Astronómico Nacional (IGN), C/ Alfonso XII, 3, 28014 Madrid, Spain
[4] Centro de Desarrollos Tecnológicos, Observatorio de Yebes (IGN), 19141 Yebes, Guadalajara, Spain

Received 6 September 2020 / Accepted 30 September 2020

ABSTRACT

Using the Yebes 40m and IRAM 30m radio telescopes, we detected a series of harmonically related lines with a rotational constant $B_0 = 4460.590 \pm 0.001$ MHz and a distortion constant $D_0 = 0.511 \pm 0.005$ kHz towards the cold dense core TMC-1. High-level-of-theory ab initio calculations indicate that the best possible candidate is protonated tricarbon monoxide, HC_3O^+. We have succeeded in producing this species in the laboratory and observed its $J_u - J_l = 2$–1 and 3–2 rotational transitions. Hence, we report the discovery of HC_3O^+ in space based on our observations, theoretical calculations, and laboratory experiments. We derive an abundance ratio $N(C_3O)/N(HC_3O^+) \sim 7$. The high abundance of the protonated form of C_3O is due to the high proton affinity of the neutral species. The chemistry of O-bearing species is modelled, and predictions are compared to the derived abundances from our data for the most prominent O-bearing species in TMC-1.

Key words. astrochemistry – ISM: molecules – ISM: individual objects: TMC-1 – line: identification – molecular data

1. Introduction

The cold dark core TMC-1 presents an interesting carbon-rich chemistry that leads to the formation of long neutral carbon-chain radicals and their anions (see Cernicharo 2020a and references therein). Cyanopolyynes, which are stable molecules, are also particularly abundant in TMC-1 (see Cernicharo 2020b and references therein). The chemistry of this peculiar object produces a large abundance of nearly saturated species, such as CH_3CHCH_2; this species may mostly be a typical molecule of hot cores (Marcelino et al. 2007). The first polar benzenic ring, C_6H_5CN (McGuire et al. 2018), was also detected in this object, while benzene itself has only been detected to date towards post-asymptotic giant branch objects (Cernicharo et al. 2001). Hence, it has been a surprising result to see that, with an almost dominant carbon chemistry, O-bearing carbon chains such as CCO (Ohishi et al. 1991), C_3O (Matthews et al. 1984), HC_5O, and HC_7O are also produced in TMC-1 (Cordiner et al. 2017; McGuire et al. 2017). The formation path for HC_5O and HC_7O is still a mystery, as is the reason for the non-detection of HC_3O, HC_4O, and HC_6O in the same cloud. The O-bearing carbon chain HC_2O has, however, been observed in cold dense clouds (Agúndez et al. 2015a).

All long carbon chains containing oxygen that have been observed so far in interstellar clouds are neutral. Cationic species related to these oxygen-bearing neutral species are thought to play an important role in the synthesis of different neutral molecules in cold dense clouds. Moreover, it has been suggested that some of them may be sufficiently long-lived to be abundant (Petrie et al. 1993), although to date no such cation has been observed. In general, the abundance of polyatomic cations in cold interstellar clouds is relatively low because they react quickly with electrons. In addition to the widespread HCO^+ and N_2H^+, the other polyatomic cations detected in cold interstellar clouds are HCS^+ (Thaddeus et al. 1981), $HCNH^+$ (Schilke et al. 1991), HC_3NH^+ (Kawaguchi et al. 1994), HCO_2^+ (Turner et al. 1999; Sakai et al. 2008), NH_3D^+ (Cernicharo et al. 2013), $NCCNH^+$ (Agúndez et al. 2015b), H_2COH^+ (Bacmann et al. 2016), H_2NCO^+ (Marcelino et al. 2018), and HC_5NH^+ (Marcelino 2020). These species are the protonated forms of abundant neutral species. The abundance ratio between a protonated molecule and its neutral counterpart, $[MH^+]/[M]$, is sensitive to the degree of ionization and thus to various physical parameters of the cloud, as well as the formation and destruction rates of the cation (Agúndez et al. 2015b). The protonated form is mainly formed by proton transfer to the neutral and destroyed by dissociative recombination with electrons. It is interesting to note that both chemical models and observations suggest a trend in which the abundance ratio $[MH^+]/[M]$ increases with the increasing proton affinity of M (Agúndez et al. 2015b).

In this Letter, we report the detection of four harmonically related lines that belong to a molecule with a $^1\Sigma$ ground electronic state towards the cold dark core TMC-1. From microwave

⋆ Based on observations carried out with the Yebes 40m telescope (projects 19A003 and 20A014) and the Institut de Radioastronomie Millimétrique (IRAM) 30m telescope. The 40m radio telescope at Yebes Observatory is operated by the Spanish Geographic Institute (IGN, Ministerio de Transportes, Movilidad y Agenda Urbana); IRAM is supported by INSU/CNRS (France), MPG (Germany), and IGN (Spain).

laboratory experiments supported by ab initio calculations, we conclude that the carrier is HC_3O^+, the protonated form of C_3O. We present a detailed observational study of the most relevant O-bearing species in this cloud and discuss these results in the context of state-of-the-art chemical models.

2. Observations

New receivers, built as part of the Nanocosmos project[1] and installed at the Yebes 40m radio telescope, were used for the observations of TMC-1. The *Q*-band receiver consists of two HEMT (high electron mobility transistor) cold amplifiers covering the 31.0–50.3 GHz band with horizontal and vertical polarizations. Receiver temperatures vary from 22 K at 32 GHz to 42 K at 50 GHz. The spectrometers are $2 \times 8 \times 2.5$ GHz FFTs (Fast Fourier Transform) with a spectral resolution of 38.1 kHz, which provides full coverage of the *Q*-band in both polarizations. The main beam efficiency varies from 0.6 at 32 GHz to 0.43 at 50 GHz.

The observations leading to the line survey in *Q*-band towards TMC-1 ($\alpha_{J2000} = 4^h41^m41.9^s$ and $\delta_{J2000} = +25°41'27.0''$) were performed over several sessions carried out between November 2019 and February 2020. The observing procedure was frequency switching with a frequency throw of 10 MHz. The nominal spectral resolution of 38.1 kHz was used for the final spectra. The sensitivity varies along the *Q*-band between 1 and 3 mK, which is a considerable improvement over previous line surveys in the 31–50 GHz frequency range (Kaifu et al. 2004).

The IRAM 30m data come from a line survey performed towards TMC-1 and B1. These observations have been described by Marcelino et al. (2007) and Cernicharo et al. (2013).

The antenna temperature intensity scale for the two telescopes used in this work was calibrated using two absorbers at different temperatures and the atmospheric transmission model ATM (Cernicharo 1985; Pardo et al. 2001). Calibration uncertainties were adopted to be 10%. All the data have been analysed using the GILDAS package[2].

3. Results

Most of the weak lines found in our survey of TMC-1 can be assigned to known species and their isotopologues, and only a few remain unidentified (Marcelino et al., in prep.). As previously mentioned, the level of sensitivity has been increased by a factor of 5–10 with respect to previous line surveys performed with other telescopes at these frequencies (Kaifu et al. 2004). Frequencies for the unknown lines were derived by assuming a local standard of rest velocity of 5.83 km s^{-1}, a value that was derived from the observed transitions of HC_5N and its isotopologues in our line survey (Cernicharo 2020a). Our new data towards TMC-1 have allowed us to detect the anions C_3N^- and C_5N^- (Cernicharo 2020a), the cation HC_5NH^+ (Marcelino 2020), and the isomer HC_4NC of HC_5N (Cernicharo 2020b), in addition to dozens of already known molecules.

The assignment of the observed features was done using the CDMS catalogue (Müller et al. 2005) and the MADEX code (Cernicharo 2012). Within the still unidentified features in our survey, we found two lines with a harmonic relation of 5:4 between them. The precision of this ratio is better than 2×10^{-5}. Taking into account the density of lines in TMC-1, the possibility that the harmonic relation between these two lines is the result of a fortuitous agreement is very small. Moreover, we explored our data at 3 mm (Marcelino et al. 2007) and found two additional lines, the $J = 10$–9 line at 89 209.749 MHz and the $J = 11$–10 transition at 98 130.267 MHz. The frequency relation 4:5:10:11 between the four lines strongly suggests that the carrier is a linear molecule with a $^1\Sigma$ ground electronic state. The observed lines are shown in Fig. 1, and the derived line parameters are given in Table 1.

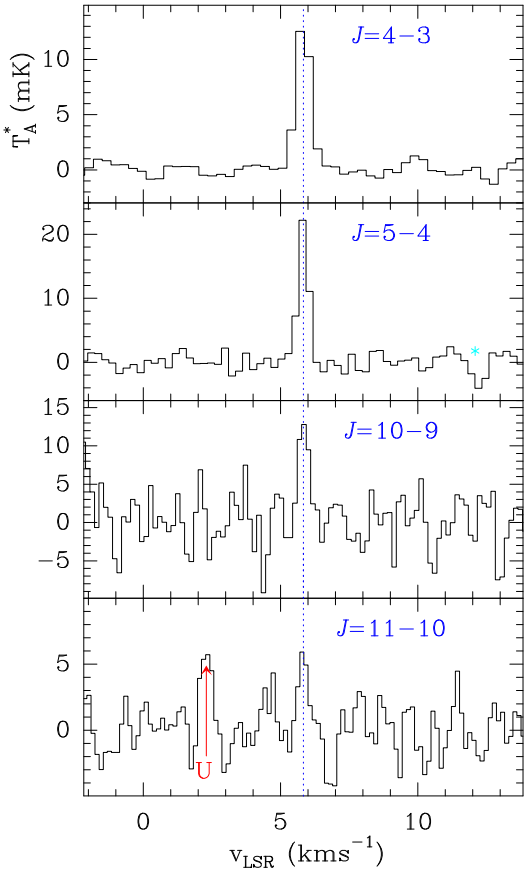

Fig. 1. Observed lines of the new molecule found in the 31–50 GHz domain towards TMC-1. The abscissa corresponds to the local standard of rest velocity in km s^{-1}. Frequencies and intensities for the observed lines are given in Table 1. The ordinate is the antenna temperature corrected for atmospheric and telescope losses in mK. The $J = 19$–18 line is only detected at a 3.5σ level. Spectral resolution is 38.1 kHz.

For a linear molecule in a $^1\Sigma$ electronic state, the frequencies of its rotational transitions follow the standard expression $\nu(J \rightarrow J-1) = 2B_0J - 4D_0J^3$. By fitting the frequencies of the lines given in Table 1, we derive $B_0 = 4460.58989 \pm 0.00096$ MHz and $D_0 = 51.06 \pm 0.47$ Hz. The standard deviation of the fit is 10.3 kHz.

3.1. Potential carriers of the series of lines

An important piece of information to know when searching for the carrier of the lines is that the $J = 4$–3 line does not show any evidence of hyperfine splitting. A molecule with a terminal CN group will produce observable hyperfine splitting for its $J = 4$–3 transition. Hence, if the molecule contains a CN group, it should be an isocyano species (-NC terminal group). The typical hyperfine quadrupole splitting of a terminal NH group will also be unresolved for the $J = 4$–3 transition.

In TMC-1, only polyatomic molecules containing H, C, N, O, and S have been found so far. In order to evaluate the possible structure of the carrier, we can consider other species that

[1] https://nanocosmos.iff.csic.es/
[2] http://www.iram.fr/IRAMFR/GILDAS

Table 1. Observed line parameters for the new molecule in TMC-1.

$J_u - J_l$	ν_{obs} [a] (MHz)	$\nu_o - \nu_c$ [b] (kHz)	$\int T_A^* dv$ [c] (mK km s^{-1})	Δv [d] (km s^{-1})	T_A^* (mK)
4–3	35684.590	−0.6	9.1 ± 0.5	0.63 ± 0.03	13.8
5–4	44605.748	+4.4	10.7 ± 0.6	0.45 ± 0.03	22.5
10–9	89209.744	−11.3	6.4 ± 1.0	0.44 ± 0.09	13.8
11–10	98130.286	8.0	2.4 ± 0.7	0.40 ± 0.10	5.8

Notes. [a]Observed frequencies adopting a v_{LSR} of 5.83 km s^{-1} for TMC-1. The uncertainty is 10 kHz for all the lines. [b]Observed minus calculated frequencies in kHz. [c]Integrated line intensity in mK km s^{-1}. [d]Line width at half intensity derived by fitting a Gaussian line profile to the observed transitions (in km s^{-1}).

have a similar rotational constant. Molecules such as HC_3N ($B_0 \sim 4549$ MHz), $HC_3^{15}N$ ($B_0 \sim 4417$ MHz), C_4H and C_4D ($B_0 \sim 4758$ MHz and 4416.4 MHz, respectively), the radical HCCCO (quasi-linear with (B+C)/2 ~4533 MHz), $NCCNH^+$ ($B_0 \sim 4438$ MHz), or H_2C_4 ($(B + C)/2 \sim 4466$ MHz) all provide a strong indication of the presence of four heavy atoms of C, N, and/or O, as well as a hydrogen or deuterium atom. Species containing sulphur, such as HCCS, HCCCS, or HNCS, have rotational constants that are very different from the observed one.

In fact, despite being an asymmetrical molecule, the species that has a close match to our rotational constant is H_2C_4; its case has to be considered in detail as its series of $J_{0,J}$ transitions are in good harmonic relation. Its lines are particularly prominent in TMC-1, $T_A^* \sim 0.2$ K. Although the measured $(B + C)/2$ value is ~6 MHz above the observed one, its isotopologues $H_2C^{13}CCC$ and $H_2CC^{13}CC$ could have a slightly lower $(B + C)/2$. Its four ^{13}C isotopologues have been observed in the laboratory (McCarthy & Thaddeus 2002). Those corresponding to the second and third carbon in the molecule have $(B + C)/2 \sim 4454.8$ and 4443.8 MHz, respectively. Hence, they do not match our B rotational constant. Moreover, taking into account the derived $^{12}C/^{13}C$ abundance ratio in TMC-1 of ~90 (Cernicharo 2020b; Taniguchi et al. 2016), the expected intensities for the four ^{13}C isotopologues of H_2C_4 are ten times weaker than the intensity of the observed lines (see Table 1 and Fig. 1). Finally, the rotational constant of the HDCCCC isotopologue is smaller than that of our series of lines (Kim & Yamamoto 2005).

The cationic species derived from the protonation of CCCO, $HCCCO^+$, was calculated by Botschwina (1989) to have a $^1\Sigma$ ground electronic state with $B_0 = 4454 \pm 10$ MHz. Recently, Thorwirth et al. (2020) performed high-level ab initio calculations and derived a rotational constant $B_0 \sim 4460.4$ MHz, which matches our observed value very well. This species may be formed from the reaction of C_3O with cations such as H_3^+ and HCO^+. The proton affinity of C_3O was calculated by Botschwina (1989) to be quite high, 885 ± 5 kJ mol^{-1}. From the observed trend of increasing protonated-to-neutral abundance ratios with increasing proton affinity (Agúndez et al. 2015b), a high abundance ratio HC_3O^+/C_3O is expected.

Although HC_3O^+ seems to be the best candidate, we have to explore other possible species derived from the isomers of $NCCNH^+$, which also has a very close rotational constant of 4438.012 MHz (Gottlieb et al. 2000). In particular, $CNCNH^+$, the protonated form of CNCN, which has also been found in space (Agúndez et al. 2018), could also be a good candidate. Other isomers with the proton on the terminal carbon atom are possible candidates as well (see Table 2). The protonated forms of the isomers of HC_3N – $HCCNCH^+$ and $HNCCCH^+$ – could also have rotational constants around the observed value. The neutral isomers of cyanoacetylene have been observed towards TMC-1 and are abundant (see Cernicharo 2020b and references therein), and the protonated form of HC_3N has also been detected in this source (see Marcelino 2020 and references therein).

Table 2. Rotational constants and electric dipole moments of potential candidates.

Molecule	B_0 (MHz)	D (kHz)	μ [a] (D)
New species [b]	4460.6	0.510	
HC_3O^+ [c]	4460.5	0.469	3.41
$HCNCN^+$ [d]	4792.8	0.554	8.33
$HNCNC^+$ [d]	4899.1	0.511	3.96
$HCNNC^+$ [d]	5210.8	0.611	6.17
$HCCNCH^+$ [d]	4646.4	0.458	3.45
$HNCCCH^+$ [d]	4327.0	0.395	1.15
$HCCCO^-$ [d]	4246.8	0.311	0.31

Notes. [a]Dipole moment calculated at the CCSD(T)-F12/cc-pCVTZ-F12 level of theory. [b]Values derived from the frequencies observed in TMC-1 (see Sect. 3). [c]B_0 and D values scaled by the ratio Exp/Calc. of the corresponding parameter HC_3N species (see Table 3). [d]All the parameters for these species have been calculated at the CCSD(T)-F12/cc-pCVTZ-F12 level of theory. No corrections using scaling factors have been applied.

3.2. Quantum chemical calculations and assignment to HC_3O^+

In order to obtain precise geometries and spectroscopic molecular parameters that help in the assignment of the observed lines, we carried out high-level ab initio calculations for all the species mentioned above. Table 2 shows the results from the geometry optimization calculations carried out at the CCSD(T)-F12/cc-pCVTZ-F12 level of theory (Raghavachari et al. 1989; Adler et al. 2007; Knizia et al. 2009; Hill et al. 2010; Hill & Peterson 2010). This method has been proven to be suitable for accurately reproducing the molecular geometry of analogue molecules (Cernicharo et al. 2019; Marcelino 2020). As can be seen, $HCNCN^+$, $HNCNC^+$, $HCNNC^+$, and $HCCNCH^+$ all have rotational constants much larger than those derived from the frequencies observed in TMC-1. Hence, they can be excluded as carriers of the observed lines.

The B_e value obtained for HC_3O^+ is 4457.383 MHz (see Table 3), which is very close to that derived for the new molecule. To obtain a more precise value for the rotational constant for HC_3O^+, we should estimate B_0 by the zero-point vibrational contribution to the rotational constant and then calibrate this value using an experimental over theoretical ratio as scaling factor for analogue molecular species. At this point, two options are possible: C_3O, which shares practically the same molecular structure, or HC_3N, which is an isoelectronic species of HC_3O^+. Structural calculations at the CCSD(T)-F12/cc-pCVTZ-F12 level of theory give a B_e value for C_3O of 4795.4 MHz, not very close to the experimental one of 4810.885 (33) (Brown et al. 1983). This discrepancy may be attributed to the floppy nature of C_3O, for which large zero-point vibrational contributions are expected (Botschwina & Reisenauer 1991). For this reason, C_3O is not a good reference system to calibrate the HC_3O^+ calculations, and, as such, we used HC_3N for this purpose. Table 3 shows the results for our calculations for HC_3N and those for HC_3O^+. After adding zero-point vibrational contribution to the B_e rotational constant and scaling by the ratio

Table 3. Theoretical values for the spectroscopic parameters of HC_3O^+ (all in MHz).

	HC_3N		HC_3O^+		
Parameter	Calc. [a]	Exp. [b]	Calc. [a]	Scaled. [c]	Scaled. [d]
B_e	4549.911		4457.383		
Vib-Rot. Corr.	4.899		1.630		
B_0	4544.215	4549.058558(40)	4455.753	4460.502	4460.443
$D \times 10^{-3}$	0.501	0.5442223(91)	0.432	0.469	0.471

Notes. [a]This work; the B_0 rotational constant has been estimated using the B_e value calculated at the CCSD(T)-F12/cc-pCVTZ-F12 level of theory and corrected with vibration-rotation interaction estimated at the MP2/cc-pVTZ level of theory. The centrifugal distortion constant has been calculated at the MP2/cc-pVTZ level of theory. [b]Thorwirth et al. (2000). [c]This work; scaled by the ratio Exp/Calc. of the corresponding parameter for the HC_3N species. [d]Thorwirth et al. (2020).

Experimental/Calculated for HC_3N, we obtained a B_0 for HC_3O^+ of 4460.502 MHz, which agrees perfectly with that derived from the TMC-1 lines. The centrifugal distortion value, obtained in the same manner but at the MP2/cc-pVTZ level of theory, is 0.469 kHz, which is compatible with that obtained from the fit of the lines. The results of our calculations are in agreement with those obtained by Thorwirth et al. (2020), which are also shown in Table 3. Finally, another potential candidate is HC_3O^-. However, our calculations indicate a rotational constant ~210 MHz below the observed one and a very low permanent dipole moment (see Table 3). Hence, from the arguments provided in the previous section and our calculations, we conclude that the best candidate for the carrier of the observed lines is HC_3O^+.

3.3. Laboratory detection of HC_3O^+

In order to confirm our assignment of the astrophysical lines to HC_3O^+, we measured its microwave spectrum using a Balle-Flygare-type Fourier transform microwave (FTMW) spectrometer combined with a pulsed discharge nozzle (Endo et al. 1994; Cabezas et al. 2016), which has been used in the past to characterize other highly reactive molecules. The reactive transient species, HC_3O^+, was produced in a supersonic expansion by a pulsed electric discharge of a gas mixture of C_2H_2 (0.15%), CO (0.8%), and H_2 (1.0%) diluted in Ne, and with the application of a voltage of 800 V through the throat of the nozzle source. We searched for the $J = 2$–1 and 3–2 rotational transitions of HC_3O^+, predicting their frequencies from the rotational constants derived in TMC-1. These frequency regions were scanned and two lines were observed, within a few kilohertz of the predicted frequencies, at 17 842.3387 and 26 763.4749 MHz with an uncertainty of 5 kHz (see Fig. 2). The following experimental results confirm that these lines belong to a transient species: (i) they disappear in the absence of electric discharge and (ii) the lines disappear when one of the reactants (C_2H_2 or CO) is removed from the gas mixture. No more lines at lower or higher frequencies ($J_u - J_l = 1$–0 and 4–3) could be observed due to the spectrum weakness and the worse performance of the spectrometer at those frequencies.

We definitively conclude that the carrier of the observed lines is protonated tricarbon monoxide (HC_3O^+). By merging the laboratory and astrophysical data, we derive
$B_0 = 4460.58896 \pm 0.00057$ MHz,
$D_0 = 50.64 \pm 0.30$ Hz,
which are the recommended constants for predicting the rotational spectrum of HC_3O^+. The standard deviation of the merged fit is 9.1 kHz. Frequency predictions have uncertainties ≤10 kHz for transitions below 100 GHz and ≤100 kHz for those in the range 100–180 GHz (see Table A.3).

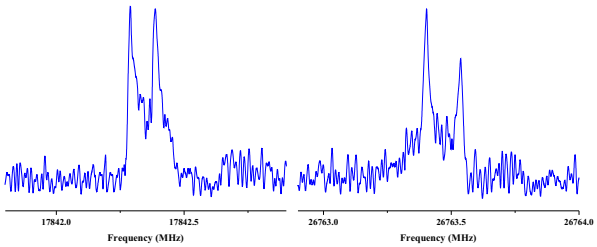

Fig. 2. FTMW spectra of HC_3O^+ showing the 2–1 and 3–2 rotational transitions at 17 842.3387 and 26 763.4695 MHz, respectively. The spectra were achieved via 20 000 shots of accumulation at a repetition rate of 10 Hz. The coaxial arrangement of the adiabatic expansion and the resonator axis produces an instrumental Doppler doubling. The resonance frequencies are calculated as the average of the two Doppler components.

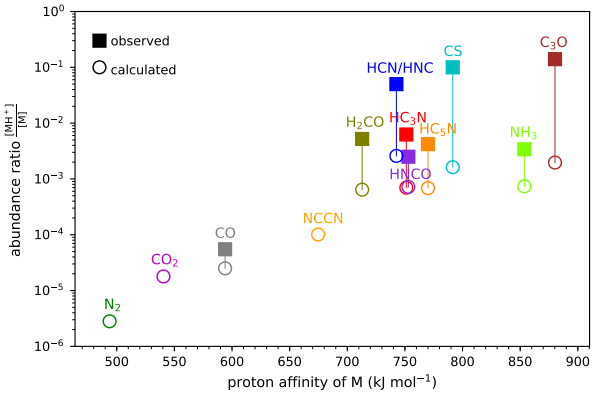

Fig. 3. Observed and calculated abundance ratios $[MH^+]/[M]$ in cold dense clouds as a function of the proton affinity of the neutral M. They are based on Agúndez et al. (2015b), with updates for H_2COH^+ from Bacmann et al. (2016), for H_2NCO^+ from Marcelino et al. (2018), for HC_5NH^+ from Marcelino (2020), and for HC_3O^+ from this study.

4. Discussion

The detection of HC_3O^+ in TMC-1 provides a further clue regarding the chemistry of protonated molecules in cold dense clouds. Agúndez et al. (2015b) find a trend in which the abundance ratio MH^+/M increases with the increasing proton affinity of the neutral M. The C_3O species has a very large proton affinity, ~885 ± 5 kJ mol^{-1} (Botschwina 1989). In

fact, it is one of the largest proton affinities among abundant molecules in cold dark clouds. The observed abundance ratio $N(HC_3O^+)/N(C_3O) = 0.14$ (see Appendix A and Table A.1) fits well with the expected value for a molecule with such a large proton affinity, according to the trend shown in Fig. 3. However, chemical model calculations similar to those presented in Agúndez et al. (2015b) predict an abundance ratio HC_3O^+/C_3O of only 2×10^{-3} at steady state, which is almost two orders of magnitude below the observed value. Part of the discrepancy may stem from the fact that rate constants for the main reactions of the formation (proton transfer from H_3O^+, HCO^+, and H_3^+) and destruction (dissociative recombination with electrons) of HC_3O^+ are not known, and thus chemical networks like UMIST RATE12 (McElroy et al. 2013) and KIDA `kida.uva.2014` (Wakelam et al. 2015a) adopt estimates for them. These estimates, however, should not be drastically different from the real ones. In general, protonated-to-neutral abundance ratios are underestimated by chemical models, probably because chemical networks miss important formation routes for the cation (see Agúndez et al. 2015b and Fig. 3). In the case of HC_3O^+, additional formation routes may be provided by reactions of the ions $C_3H_2^+$ and linear $C_3H_3^+$ with O atoms, which is currently not considered in the aforementioned reaction networks. The reaction between $C_4H_2^+$ and O atoms (e.g. Tenenbaum et al. 2006) is only an efficient route to HC_3O^+ at very early times ($<10^5$ yr), while reactions of C_3H^+ with O_2, H_2O, and CO_2 (Herbst et al. 1984) are not a major route to HC_3O^+ according to the chemical model. The sulphur analogue HC_3S^+ is a good candidate for detection given that C_3S has a very high proton affinity (933 kJ mol^{-1}) and is around five times more abundant than C_3O. We searched for it in our line survey using the ab initio calculations of Thorwirth et al. (2020) and derive an upper limit to its column density of 3×10^{11} cm^{-2}, which implies an abundance ratio $N(HC_3S^+)/N(C_3S) < 0.04$. The lower MH^+/M ratio of C_3S compared to C_3O probably stems from the fact that routes to HC_3O^+ involving O atoms can be efficient because of the high abundance of neutral O atoms, while the sulphur analogous routes would be less efficient because atomic sulphur is expected to be preferably in ionized rather than neutral form.

In Table A.1, we present a comprehensive list of abundances derived from our data for O-bearing molecules in TMC-1. The chemistry of some of these species has already been discussed in detail, for example, in Agúndez et al. (2015a) and Wakelam et al. (2015b) for HCCO, in Loison et al. (2016) for the isomers *c*-H_2C_3O and HCCCHO, and in McGuire et al. (2017) and Cordiner et al. (2017) for HC_5O and HC_7O. These last O-bearing carbon chains deserve some discussion. They represent a new class of interstellar molecules and their chemistry is not yet well understood. Cordiner & Chamley (2012) proposed that HC_nO molecules may directly form through reactions of hydrocarbon anions C_nH^- with O atoms in a process of associative electron detachment. This mechanism, however, overestimates the abundances of HC_6O, C_6O, and C_7O by one to two orders of magnitude (Cordiner et al. 2017). McGuire et al. (2017) proposed that HC_nO molecules could form through radiative association reactions of $C_nH_2^+$ and $C_nH_3^+$ ions with CO followed by dissociative recombination with electrons. This mechanism explains the non-detection of HC_6O in terms of a low reactivity between $C_5H_2^+$ and CO (Adams et al. 1989), although it overestimates the abundance of HC_4O by almost two orders of magnitude. The large abundance found for HC_3O^+ suggests that reactions between hydrocarbon ions and atomic oxygen probably participate in the growth of these long O-bearing carbon chains.

Acknowledgements. The Spanish authors thank Ministerio de Ciencia e Innovación for funding support through projects AYA2016-75066-C2-1-P, PID2019-107115GB-C21. We also thank ERC for funding through Grant ERC-2013-Syg-610256-NANOCOSMOS. M. A. and C. B. thanks MICIN for grants RyC-2014-16277 and FJCI-2016-27983, respectively. Y. Endo thanks Ministry of Science and Technology of Taiwan through Grant MOST108-2113-M-009-25.

References

Adler, T. B., Knizia, G., & Werner, H.-J. 2007, J. Chem. Phys., 127, 221106
Adams, N. G., Smith, D., Giles, K., & Herbst, E. 1989, A&A, 220, 269
Agúndez, M., Cernicharo, J., & Guélin, M. 2015a, A&A, 577, L5
Agúndez, M., Cernicharo, J., de Vicente, P., et al. 2015b, A&A, 579, L10
Agúndez, M., Marcelino, N., & Cernicharo, J. 2018, ApJ, 861, L22
Bacmann, A., García-García, E., & Faure, A. 2016, A&A, 588, L8
Botschwina, P. 1989, J. Chem. Phys., 90, 4301
Botschwina, P., & Reisenauer, H. P. 1991, Chem. Phys. Lett., 183, 217
Brown, R. D., Eastwood, F. W., Elmes, P. S., & Godfrey, P. D. 1983, J. Am. Chem. Soc., 105, 6496
Cabezas, C., Guillemin, J.-C., & Endo, Y. 2016, J. Chem. Phys., 145, 184304
Cernicharo, J. 1985, Internal IRAM report (Granada: IRAM)
Cernicharo, J. 2012, EAS Pub. Ser., 2012, 251, `https://nanocosmos.iff.csic.es/?page_id=1619`
Cernicharo, J., & Guélin, M. 1987, A&A, 176, 299
Cernicharo, J., Heras, A. M., Tielens, A. G. G. M., et al. 2001, ApJ, 546, L123
Cernicharo, J., Tercero, B., Fuente, A., et al. 2013, ApJ, 771, L10
Cernicharo, J., Cabezas, C., Pardo, J. R., et al. 2019, A&A, 630, L2
Cernicharo, J., Marcelino, N., Pardo, J. R., et al. 2020a, A&A, 641, L9
Cernicharo, J., Marcelino, N., Agundez, M., et al. 2020b, A&A, 642, L8
Cordiner, M. A., & Chamley, S. B. 2012, ApJ, 749, 120
Cordiner, M. A., Chamley, S. B., Kisiel, Z., et al. 2017, ApJ, 850, 187
Endo, Y., Kohguchi, H., & Ohshima, Y. 1994, Faraday Discuss., 97, 341
Fossé, D., Cernicharo, J., Gerin, M., & Cox, P. 2001, ApJ, 552, 168
Gottlieb, C. A., Aponi, A. J., McCarthy, M. C., & Thaddeus, P. 2000, J. Chem. Phys., 113, 1910
Herbst, E., Smith, D., & Adams, N. G. 1984, A&A, 138, L13
Hill, J. G., & Peterson, K. A. 2010, Phys. Chem. Chem. Phys., 12, 10460
Hill, J. G., Mazumder, S., & Peterson, K. A. 2010, J. Chem. Phys., 132, 054108
Kaifu, N., Ohishi, M., Kawaguchi, K., et al. 2004, PASJ, 56, 69
Kawaguchi, K., Kasai, Y., Ishikawa, S., et al. 1994, ApJ, 420, L95
Kim, E., & Yamamoto, S. 2005, J. Mol. Spectrosc., 233, 93
Knizia, G., Adler, T. B., & Werner, H.-J. 2009, J. Chem. Phys., 130, 054104
Loison, J.-C., Agúndez, M., Marcelino, N., et al. 2016, MNRAS, 456, 4101
Matthews, H. E., Irvine, E., Friberg, F. M., et al. 1984, Nature, 310, 125
Marcelino, N., Cernicharo, J., Agúndez, M., et al. 2007, ApJ, 665, L127
Marcelino, N., Agúndez, M., Cernicharo, J., et al. 2018, A&A, 612, L10
Marcelino, N., Agundez, M., Tercero, B., et al. 2020, A&A, in press, `https://doi.org/10.1051/0004-6361/202039251`
McCarthy, M. C., & Thaddeus, P. 2002, J. Mol. Spectrosc., 211, 235
McElroy, D., Walsh, C., Markwick, A. J., et al. 2013, A&A, 550, A36
McGuire, B. A., Burkhardt, M., Shingledecker, C. N., et al. 2017, ApJ, 843, L28
McGuire, B. A., Burkhardt, M., Kalenskii, S., et al. 2018, Science, 359, 202
Müller, H. S. P., Schlöder, F., Stutzki, J., & Winnewisser, G. 2005, J. Mol. Struct., 742, 215
Ohishi, M., Suzuki, H., Ishikawa, S.-I., et al. 1991, ApJ, 380, L39
Pardo, J. R., Cernicharo, J., & Serabyn, E. 2001, IEEE Trans. Antennas Propag., 49, 12
Petrie, S., Bettens, R. P. A., Freeman, C. G., & McEwan, M. J. 1993, MNRAS, 264, 862
Raghavachari, K., Trucks, G. W., Pople, J. A., & Head-Gordon, M. 1989, Chem. Phys. Lett., 157, 479
Sakai, N., Sakai, T., Aikawa, Y., & Yamamoto, S. 2008, ApJ, 675, L89
Schilke, P., Walmsley, C. M., Millar, T. J., & Henkel, C. 1991, A&A, 247, 487
Taniguchi, K., Ozeki, H., Saito, M., et al. 2016, ApJ, 817, 147
Tenenbaum, E. D., Apponi, A. J., Ziurys, L. M., et al. 2006, ApJ, 649, L17
Thaddeus, P., Guélin, M., & Linke, R. A. 1981, ApJ, 246, L41
Thorwirth, S., Müller, H. S. P., & Winnewisser, G. 2000, J. Mol. Spectrosc., 204, 133
Thorwirth, S., Harding, M. E., Asvany, O., et al. 2020, Mol. Phys., in press, `https://doi.org/10.1080/00268976.2020.1776409`
Turner, B. E., Terzieva, R., & Herbst, E. 1999, ApJ, 518, 699
Wakelam, V., Loison, J.-C., Herbst, E., et al. 2015a, ApJS, 217, 20
Wakelam, V., Loison, J.-C., Hickson, K. M., & Ruaud, M. 2015b, MNRAS, 453, L48

Appendix A: Observational data for O-bearing species in TMC1

Table A.1. Column densities for relevant O-bearing species in TMC-1.

Molecule	N [a]	X [b]	$N(CH_3OH)/N$	
$HCCCO^+$	$2.1(2)\times10^{11}$	2.1×10^{-11}	229	
$HOCO^+$	$4.0(2)\times10^{11}$	4.0×10^{-11}	120	
H_2COH^+	$\leq3.0\times10^{11}$	$\leq3.0\times10^{-11}$	$\geq$160	
H_2NCO^+	$\leq4.0\times10^{10}$	$\leq4.0\times10^{-12}$	$\geq$1200	
HNCO	$1.3(1)\times10^{13}$	1.3×10^{-9}	3.7	
HCNO	$7.0(3)\times10^{10}$	7.0×10^{-12}	686	
HOCN	$1.1(2)\times10^{11}$	1.1×10^{-11}	437	
CH_3OH	$4.8(3)\times10^{13}$	4.8×10^{-9}	1	$A+E$
CCO	$1.5(3)\times10^{12}$	1.5×10^{-10}	32	
CCCO	$1.5(2)\times10^{12}$	1.5×10^{-10}	32	
CCCCO	$\leq1.2\times10^{11}$	$\leq1.2\times10^{-11}$	$\geq$400	
CCCCCO	$\leq4.0\times10^{10}$	$\leq4.0\times10^{-12}$	$\geq$1200	
HCOOH	$1.4(2)\times10^{12}$	1.4×10^{-10}	34	
HCCO	$1.0(2)\times10^{12}$	1.0×10^{-10}	48	
HCCCO	$\leq2.0\times10^{11}$	$\leq2.0\times10^{-11}$	$\geq$240	
HCCCCO	$\leq3.0\times10^{11}$	$\leq3.0\times10^{-11}$	$\geq$160	
HCCCCCO	$1.8(2)\times10^{12}$	1.8×10^{-10}	27	
HCCCCCCO	$\leq7.0\times10^{11}$	$\leq7.0\times10^{-11}$	$\geq$59	
HCCCCCCCO	$\leq9.0\times10^{11}$	$\leq9.0\times10^{-11}$	$\geq$53	
H_2CCO	$1.4(2)\times10^{13}$	1.4×10^{-9}	3.4	$o+p$
H_2CCCO	$\leq1.1\times10^{11}$	$\leq1.1\times10^{-11}$	$\geq$436	
c-H_2C_3O	$4.0(2)\times10^{11}$	4.0×10^{-11}	120	$o+p$
HCCCHO	$2.0(2)\times10^{12}$	2.0×10^{-10}	240	
H_2CCCCO	$\leq1.2\times10^{11}$	$\leq1.2\times10^{-11}$	$\geq$400	o
CH_3CHO	$3.5(2)\times10^{12}$	3.5×10^{-10}	14	$A+E$
NH_2CHO	$\leq5.0\times10^{10}$	$\leq5.0\times10^{-12}$	$\geq$960	
HCCCCOH	$\leq1.0\times10^{11}$	$\leq1.0\times10^{-11}$	$\geq$480	

Notes. [a]Column density in cm^{-2}. Upper limits correspond to 3σ values. [b]Relative abundance to H_2 assuming a total column density of molecular hydrogen of 10^{22} cm^{-2} (Cernicharo & Guélin 1987).

In order to study the chemistry of O-bearing species in TMC-1, we explored the lines arising from these species in our line survey. The derived line parameters are given in Table A.2, and some selected lines are shown in Fig. A.1. Line parameters were derived by fitting a Gaussian line profile to the observed features. Rest frequencies were adopted from the MADEX code (Cernicharo 2012). In order to derive column densities, we assumed that all molecular species are thermalized at a temperature of 10 K. Main beam efficiency (see Sect. 2) and source dilution in the beam were applied to all the observations. For the source dilution, we assumed a source radius of 40″ (Fossé et al. 2001), that is to say, the source practically fills the main beam of the telescope at all observed frequencies. The derived column densities of detected O-bearing species in our survey were obtained using the MADEX code and are given in Table A.1. The 1σ sensitivity of the survey is ~0.6–0.7 mK and 0.7–2.0 mK below and above 40 GHz, respectively. Hence, the data allow us to derive very sensitive 3σ upper limits for the column density of many O-bearing species, which are given in Table A.1. It is worth noting that although many lines of HC_5O are detected in our survey, only upper limits have been obtained for HC_7O lines, which has been reported previously by McGuire et al. (2017) and Cordiner et al. (2017) using line stacking.

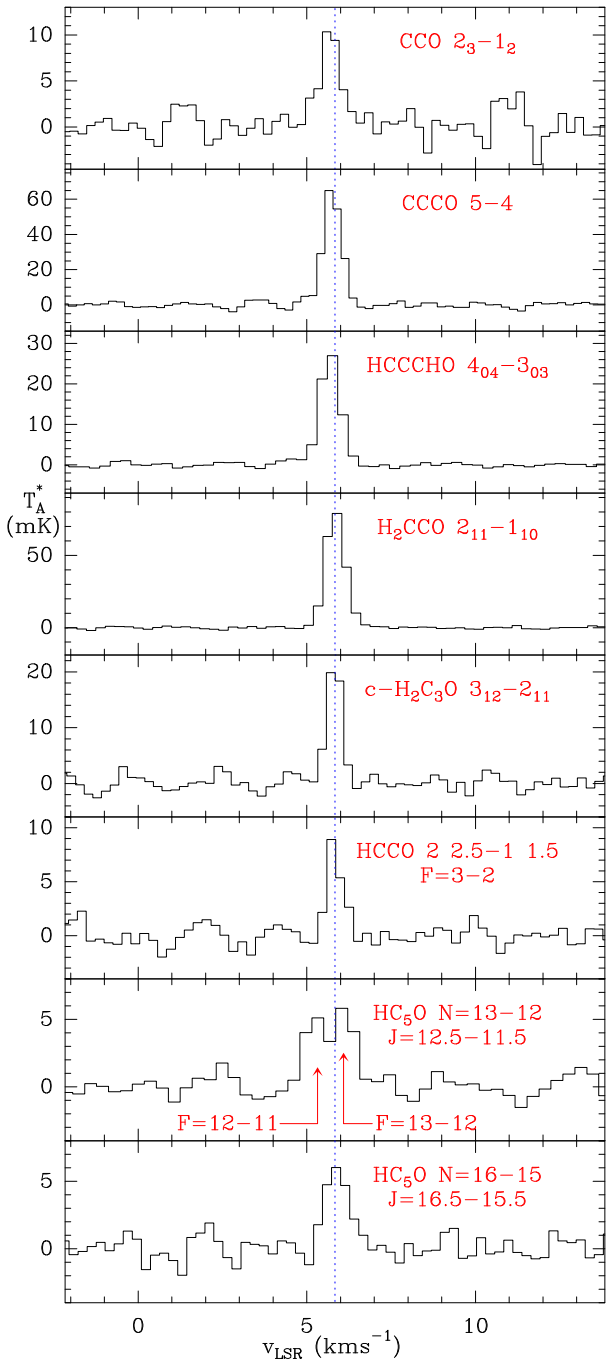

Fig. A.1. Selected lines of O-bearing species observed towards TMC1 in the 31–50 GHz domain. The abscissa corresponds to the local standard of rest velocity in $km\,s^{-1}$. Frequencies and intensities for the observed lines are given in Table A.2. The ordinate is the antenna temperature corrected for atmospheric and telescope losses in mK. Spectral resolution is 38.1 kHz.

Table A.3 provides the frequencies, uncertainties, upper energy levels, Einstein coefficients, and degeneracies for transitions up to $J = 30$–29. This information is provided with the intent of facilitating the search for HC_3O^+ in other sources and with other instruments.

Table A.2. Derived line parameters for O-bearing species in TMC-1.

Molecule	Transition	$\nu_{\rm rest}$ [a] (MHz)	$\int T_A^* dv$ [b] (mK km s^{-1})	$v_{\rm LSR}$ [c] (km s^{-1})	Δv [d] (km s^{-1})	T_A^* [e] (mK)
CCO	1_1–0_1	32 623.449 ± 0.007	5.1 ± 0.7	5.57(05)	1.09(13)	4.5
CCO	2_1–1_1	32 738.613 ± 0.005	1.6 ± 0.7	6.33(18)	1.46(34)	1.0
CCO	2_3–1_2	45 826.734 ± 0.002	8.1 ± 0.9	5.69(04)	0.73(11)	10.0
CCO	2_2–1_1	46 182.187 ± 0.002	2.5 ± 1.0	5.73(17)	0.89(31)	2.7
CCCO	4–3	38 486.891 ± 0.001	43.5 ± 1.0	5.74(01)	0.63(07)	64.5
CCCO	5–4	48 108.474 ± 0.001	44.2 ± 1.0	5.75(01)	0.63(14)	66.4
HNCO	2_{02}–1_{01} 1–1	43 962.007 ± 0.030	20.1 ± 1.0	5.76(01)	0.62(02)	35.1
HNCO	2_{02}–1_{01} 1–2	43 962.641 ± 0.006				≤2.7
HNCO	2_{02}–1_{01} 3–2	43 963.000 ± 0.030	178.8 ± 1.0	5.76(01)	0.68(01)	247.8
HNCO	2_{02}–1_{01} 2–1	43 963.000 ± 0.030				
HNCO	2_{02}–1_{01} 1–0	43 963.626 ± 0.030	26.1 ± 2.0	6.35(02)	0.60(04)	41.2
HNCO	2_{02}–1_{01} 2–2	43 963.626 ± 0.030	22.9 ± 2.0	5.66(03)	0.64(05)	33.6
HCNO	2–1	45 876.069 ± 0.002	7.1 ± 1.0	5.79(08)	0.98(16)	6.9
HOCN	2_{02}–1_{01}	41 950.836 ± 0.001	13.6 ± 1.0	5.55(02)	0.82(03)	15.6
HCOOH	2_{12}–1_{11}	43 303.705 ± 0.001	3.4 ± 0.5	6.10(09)	0.61(10)	5.2
HCOOH	2_{02}–1_{01}	44 911.734 ± 0.001	6.7 ± 0.5	5.82(05)	0.79(10)	7.9
HCOOH	2_{11}–1_{10}	46 581.220 ± 0.001	2.1 ± 0.5	5.95(14)	0.70(22)	2.8
HCCCHO	4_{14}–3_{13}	36 648.266 ± 0.006	7.4 ± 0.5	5.76(02)	0.78(05)	9.0
HCCCHO	4_{04}–3_{03}	37 290.136 ± 0.006	21.0 ± 0.5	5.64(01)	0.70(02)	28.1
HCCCHO	4_{13}–3_{12}	37 954.572 ± 0.006	10.4 ± 0.5	5.59(01)	0.74(04)	13.2
HCCCHO	5_{15}–4_{14}	45 807.708 ± 0.007	3.5 ± 0.7	5.73(05)	0.46(10)	7.3
HCCCHO	5_{05}–4_{04}	46 602.868 ± 0.007	25.5 ± 0.5	5.64(01)	0.65(02)	3.6
HCCCHO	5_{14}–4_{13}	47 440.427 ± 0.007	6.0 ± 0.7	5.61(04)	0.55(09)	10.3
A-CH_3CHO	4_{04}–3_{13}	32 709.214 ± 0.002				≤1.8
A-CH_3CHO	2_{12}–1_{11}	37 464.204 ± 0.001	12.1 ± 1.0	5.84(02)	0.91(06)	12.5
A-CH_3CHO	2_{02}–1_{01}	38 512.079 ± 0.001	31.3 ± 0.6	5.85(01)	0.82(01)	35.7
A-CH_3CHO	2_{11}–1_{10}	39 594.289 ± 0.001	14.0 ± 1.0	5.83(02)	0.79(05)	16.6
A-CH_3CHO	1_{10}–1_{01}	47 820.620 ± 0.002	4.3 ± 0.6	5.76(08)	0.65(13)	6.1
A-CH_3CHO	2_{11}–2_{02}	48 902.831 ± 0.002	4.0 ± 0.6	5.76(07)	0.66(13)	5.6
E-CH_3CHO	4_{+04}–3_{-13}	33 236.468 ± 0.002				≤2.0
E-CH_3CHO	2_{-12}–1_{+10}	35 837.312 ± 0.003	1.3 ± 0.6	5.89(09)	0.62(20)	2.0
E-CH_3CHO	2_{-12}–1_{-11}	37 686.932 ± 0.002	9.7 ± 1.0	5.88(02)	0.75(05)	12.1
E-CH_3CHO	2_{+02}–1_{+01}	38 506.035 ± 0.001	33.7 ± 1.0	5.85(01)	0.82(01)	38.5
E-CH_3CHO	2_{+11}–1_{+10}	39 362.537 ± 0.002	13.8 ± 1.0	5.82(02)	0.84(04)	15.4
E-CH_3CHO	2_{+11}–1_{-11}	41 212.157 ± 0.003	2.5 ± 0.8	6.07(09)	0.83(16)	2.8
E-CH_3CHO	1_{-11}–1_{+01}	45 897.347 ± 0.003				≤3.0
E-CH_3CHO	1_{+10}–1_{+01}	47 746.968 ± 0.002	2.5 ± 0.8	6.17(22)	0.82(23)	2.8
E-CH_3CHO	2_{+11}–2_{+02}	48 603.469 ± 0.002	6.8 ± 1.0	5.88(05)	0.75(11)	8.6
o-H_2CCO	2_{12}–1_{11}	40 039.017 ± 0.001	57.8 ± 0.7	5.77(01)	0.68(01)	79.5
o-H_2CCO	2_{11}–1_{10}	40 793.842 ± 0.001	59.4 ± 0.7	5.79(01)	0.68(01)	81.9
p-H_2CCO	2_{02}–1_{01}	40 417.950 ± 0.001	37.9 ± 0.7	5.78(01)	0.64(02)	55.9
o-c-H_2C_3O	3_{13}–2_{12}	39 956.733 ± 0.004	14.9 ± 0.8	5.81(01)	0.65(03)	21.5
o-c-H_2C_3O	3_{12}–2_{11}	44 587.397 ± 0.004	12.4 ± 0.8	5.82(01)	0.51(03)	22.8
p-c-H_2C_3O	3_{03}–2_{02}	42 031.939 ± 0.004	6.4 ± 0.8	5.78(03)	0.68(07)	8.9
p-c-H_2C_3O	3_{22}–2_{21}	42 316.187 ± 0.003	1.7 ± 0.7	5.78(02)	0.27(10)	6.0
p-c-H_2C_3O	3_{21}–2_{20}	42 601.246 ± 0.003	2.4 ± 0.7	5.94(03)	0.48(09)	4.6
HCCO	2,2.5–1, 1.5 F = 3–2	43 317.673 ± 0.006	4.9 ± 0.8	5.80(03)	0.51(08)	8.9
HCCO	2,2.5–1, 1.5 F = 2–1	43 321.150 ± 0.006	3.8 ± 0.8	5.70(05)	0.67(15)	5.4
HCCO	2,1.5–1, 0.5 F = 2–1	43 329.543 ± 0.006	3.8 ± 0.8	5.67(06)	0.64(15)	5.5
HCCO	2,1.5–1, 0.5 F = 1–0	43 335.462 ± 0.004	4.2 ± 0.8	5.69(08)	0.97(17)	4.1

Notes. [a]Rest frequencies and uncertainties from MADEX (Cernicharo 2012). [b]Integrated line intensity in mK kms^{-1}. [c]Local standard of rest velocity of the observed emission kms^{-1}. [d]Line width at half intensity derived by fitting a Gaussian line profile to the observed transitions (in kms^{-1}). [e]Upper limits to the antenna temperature correspond to 3σ values. [f]Average of two hyperfine components.

Table A.2. continued.

Molecule	Transition	$\nu_{\rm rest}$ [a] (MHz)	$\int T_A^* {\rm d}v$ [b] (mK km s^{-1})	$v_{\rm LSR}$ [c] (km s^{-1})	Δv [d] (km s^{-1})	T_A^* [e] (mK)
HC_5O	13 1 12.5–12 −1 11.5 13–12	32 267.964 ± 0.002	3.7 ± 0.9	5.52(06)	0.63(09)	5.6
HC_5O	13 1 12.5–12 −1 11.5 12–11	32 268.049 ± 0.002	4.8 ± 1.0	5.65(07)	0.73(15)	6.0
HC_5O	13 −1 12.5–12 1 11.5 13–12	32 271.760 ± 0.002	2.7 ± 1.0	5.59(08)	0.62(14)	3.9
HC_5O	13 −1 12.5–12 1 11.5 12–11	32 271.848 ± 0.002	4.3 ± 1.0	5.62(06)	0.76(15)	5.4
HC_5O	14 −1 13.5–13 1 12.5 14–13	34 849.461 ± 0.002	1.9 ± 0.7	5.58(02)	0.33(16)	5.0
HC_5O	14 −1 13.5–13 1 12.5 13–12	34 849.540 ± 0.002	4.5 ± 1.0	5.67(03)	0.81(08)	5.3
HC_5O	14 1 13.5–13 −1 12.5 14–13	34 853.387 ± 0.002	4.5 ± 1.0	5.69(17)	0.74(14)	5.7
HC_5O	14 1 13.5–13 −1 12.5 13–12	34 853.469 ± 0.002	3.1 ± 0.9	5.63(14)	0.54(16)	5.4
HC_5O	15 1 14.5–14 −1 13.5 15–14 [f]	37 430.982 ± 0.003	6.3 ± 1.0	5.79(03)	0.93(05)	6.4
HC_5O	15 −1 14.5–14 1 13.5 15–14 [f]	37 435.050 ± 0.003	6.2 ± 1.0	5.79(04)	0.99(09)	5.9
HC_5O	15 −1 15.5–15 1 14.5 16–15 [f]	40 012.451 ± 0.004	5.3 ± 1.0	5.80(06)	1.00(12)	4.9
HC_5O	15 1 15.5–15 −1 14.5 16–15 [f]	40 016.668 ± 0.004	7.1 ± 1.0	5.86(04)	1.02(10)	6.5
HC_5O	16 1 16.5–15 −1 15.5 17–16 [f]	42 593.906 ± 0.004	5.2 ± 1.0	5.70(05)	0.77(09)	6.3
HC_5O	16 −1 16.5–15 1 15.5 17–16 [f]	42 598.284 ± 0.004	5.4 ± 1.0	5.89(04)	0.82(09)	6.2
HC_5O	17 −1 17.5–16 1 16.5 18–17 [f]	45 175.346 ± 0.005	5.4 ± 1.0	5.75(11)	1.05(19)	4.8
HC_5O	17 1 17.5–16 −1 16.5 18–17 [f]	45 179.895 ± 0.005	6.3 ± 1.0	5.80(08)	1.06(17)	5.6
HC_5O	18 1 18.5–17 −1 17.5 19–18 [f]	47 756.772 ± 0.007				≤5.1
HC_5O	18 −1 18.5–17 1 17.5 19–18 [f]	47 761.501 ± 0.007				≤5.1

Table A.3. Predicted frequencies of HC_3O^+.

Transition	ν (MHz)	E_{up} (K)	A_{ij} (s^{-1})	S_{ij}	g_u
1 → 0	8 921.175 ± 0.001	0.4	2.928 10^{-08}	1	3
2 → 1	17 842.338 ± 0.003	1.3	2.810 10^{-07}	2	5
3 → 2	26 763.477 ± 0.004	2.6	1.016 10^{-06}	3	7
4 → 3	35 684.579 ± 0.005	4.3	2.498 10^{-06}	4	9
5 → 4	44 605.633 ± 0.006	6.4	4.990 10^{-06}	5	11
6 → 5	53 526.627 ± 0.006	9.0	8.756 10^{-06}	6	13
7 → 6	62 447.547 ± 0.006	12.0	1.406 10^{-05}	7	15
8 → 7	71 368.383 ± 0.006	15.4	2.116 10^{-05}	8	17
9 → 8	80 289.124 ± 0.006	19.3	3.033 10^{-05}	9	19
10 → 9	89 209.754 ± 0.008	23.5	4.182 10^{-05}	10	21
11 → 10	98 130.263 ± 0.010	28.3	5.590 10^{-05}	11	23
12 → 11	107 050.638 ± 0.014	33.4	7.284 10^{-05}	12	25
13 → 12	115 970.868 ± 0.020	39.0	9.290 10^{-05}	13	27
14 → 13	124 890.942 ± 0.027	45.0	1.163 10^{-04}	14	29
15 → 14	133 810.844 ± 0.035	51.4	1.434 10^{-04}	15	31
16 → 15	142 730.566 ± 0.045	58.2	1.744 10^{-04}	16	33
17 → 16	151 650.094 ± 0.056	65.5	2.095 10^{-04}	17	35
18 → 17	160 569.416 ± 0.069	73.2	2.491 10^{-04}	18	37
19 → 18	169 488.521 ± 0.083	81.3	2.934 10^{-04}	19	39
20 → 19	178 407.395 ± 0.099	89.9	3.427 10^{-04}	20	41
21 → 20	187 326.026 ± 0.118	98.9	3.971 10^{-04}	21	43
22 → 21	196 244.404 ± 0.138	108.3	4.571 10^{-04}	22	45
23 → 22	205 162.515 ± 0.160	118.2	5.227 10^{-04}	23	47
24 → 23	214 080.348 ± 0.185	128.4	5.944 10^{-04}	24	49
25 → 24	222 997.889 ± 0.211	139.1	6.724 10^{-04}	25	51
26 → 25	231 915.129 ± 0.240	150.3	7.569 10^{-04}	26	53
27 → 26	240 832.053 ± 0.272	161.8	8.482 10^{-04}	27	55
28 → 27	249 748.650 ± 0.306	173.8	9.466 10^{-04}	28	57
29 → 28	258 664.908 ± 0.342	186.2	1.052 10^{-03}	29	59
30 → 29	267 580.815 ± 0.381	199.1	1.166 10^{-03}	30	61